Calculation of the cumulative reaction probability via a discrete variable representation with absorbing boundary conditions

Tamar Seideman and William H. Miller
Department of Chemistry, University of California, Berkeley, California 94720

(Received 13 November 1991; accepted 9 December 1991)

A new method is suggested for the calculation of the microcanonical cumulative reaction probability *via* flux autocorrelation relations. The Hamiltonian and the flux operators are computed in a discrete variable representation (DVR) and a well-behaved representation for the Green's operator, $G(E^+)$, is obtained by imposing absorbing boundary conditions (ABC). Applications to a one-dimensional-model problem and to the collinear $H + H_2$ reaction show that the DVR-ABC scheme provides a very efficient method for the *direct* calculation of the microcanonical probability, circumventing the need to compute the state-to-state dynamics. Our results indicate that the cumulative reaction probability can be calculated to a high accuracy using a rather small number of DVR points, confined to the vicinity of the transition state. Only limited information regarding the potential-energy surface is therefore required, suggesting that this method would be applicable also to higher dimensionality problems, for which the complete potential surface is often unknown.

I. INTRODUCTION

It is well recognized that only a quantum-mechanical scattering calculation provides *all* the attributes of a bimolecular chemical reaction, i.e., state-to-state differential and integral cross sections. However, one is often interested in much less detailed quantities, e.g., the thermally averaged rate constant for the reaction. There is thus considerable interest in theoretical approaches that allow one to calculate the rate constant *directly*, i.e., without having to first solve the complete state-to-state reactive scattering problem, but nevertheless *rigorously*.

Reactive flux correlation functions do, in fact, provide a means for such a direct calculation.[1,2] Most of the recent effort along these lines has focused on the flux–flux autocorrelation function[3–8]

$$C_f(t) = \mathrm{tr}\left[Fe^{iHt_c^*/\hbar}Fe^{-iHt_c/\hbar}\right], \tag{1.1a}$$

the time integral of which gives the rate constant

$$k(T) = Q_r(T)^{-1}\int_0^\infty dt C_f(t). \tag{1.1b}$$

[H in Eq. (1.1a) is the total Hamiltonian of the molecular system, F a flux operator (see Sec. II), $t_c = t - i\hbar/2kT$, T the temperature, Q_r the reactant partition function per unit volume, and tr denotes a quantum mechanical trace.] This paper, however, deals with a direct calculation of the *cumulative reaction probability*, $N(E)$, the Boltzmann average of which gives the thermal rate constant,

$$k(T) = [2\pi\hbar Q_r(T)]^{-1}\int_{-\infty}^{\infty} dE e^{-E/kT}N(E), \tag{1.2}$$

where E is the total energy of the molecular system. In some cases, usually for *unimolecular* reactions, one is interested in the *microcanonical* rate constant, which is given in terms of $N(E)$ by

$$k(E) = [2\pi\hbar\rho_r(E)]^{-1}N(E), \tag{1.3}$$

where ρ_r is the density of reactant states per unit energy.

The primary definition of the cumulative reaction probability is as the sum of reaction probabilities (squares of S-matrix elements) over all internal (rotational and vibrational) states of reactants and products[9]

$$N(E) = \sum_{\mathbf{n}_r,\mathbf{n}_p} |S_{\mathbf{n}_r\mathbf{n}_p}(E)|^2, \tag{1.4}$$

where $\mathbf{n}_r$ and $\mathbf{n}_p$ denote the collection of asymptotic quantum numbers of the reactants and products, respectively. Although one can calculate $N(E)$ via Eq. (1.4) once a reactive scattering calculation has been carried out to obtain the S matrix, it obviously does not provide a *direct* approach to $N(E)$ because one must first obtain all the state-to-state information (i.e., the S matrix) which is then averaged to obtain $N(E)$. There does, however, exist a "direct" expression for $N(E)$, derived from the flux correlation function analysis,[2(b)]

$$N(E) = \tfrac{1}{2}(2\pi\hbar)^2\mathrm{tr}[F\delta(E-H)F\delta(E-H)], \tag{1.5a}$$

the evaluation of which is the subject of this paper. F in Eq. (1.5a) is the same flux operator as in Eq. (1.1a), and the microcanonical density operator is usually obtained from the outgoing wave Green's function

$$\delta(E-H) = -\frac{1}{\pi}\mathrm{Im}\,G(E^+) = -\frac{1}{\pi}\mathrm{Im}\lim_{\epsilon\to 0}(E+i\epsilon-H)^{-1}. \tag{1.5b}$$

Equation (1.5) is equivalent to Eq. (1.4), but it has the advantage of no reference to asymptotic quantum states.

Thirumalai, Garrett, and Berne[10(a)] have previously attacked the evaluation of Eq. (1.5a) using a finite Gaussian approximation for the δ-function operator [i.e., $\delta(z)$

 0021-9606/92/064412-11$06.00

$\approx\sqrt{\beta/\pi}\exp(-\beta z^2)$, with $z=E-H$ and β sufficiently large], and McCurdy and Garrett[10(b)] have used a finite difference approach to solve the Schrödinger equation for $G(E^+)$ and obtain the microcanonical density operator via Eq. (1.5b). We have recently shown how $G(E^+)$ can be determined in terms of Siegert eigenvalues associated with the transition state, i.e., the saddle-point region of the potential-energy surface.[11] Although these works treated only one-dimensional examples, they nevertheless showed that it is indeed possible to evaluate $N(E)$ directly, i.e., via Eq. (1.5). In addition, work by Lefebvre and Moiseyev[7] using complex scaling/coordinate rotation methods could also be modified to compute $G(E^+)$ and thus $N(E)$ via Eq. (1.5).

In this paper we report what we believe to be significant progress in the search for an efficient and systematic approach for the direct evaluation of $N(E)$ via Eq. (1.5). The two key elements that we bring to bare on the problem are the use of a discrete variable representation[12-16] (DVR) as the basis set in which the Hamiltonian and flux operator in Eq. (1.5) are represented and the trace carried out, and the use of absorbing boundary conditions[17-21] (ABC) to give a well-behaved representation of the operator $G(E^+)$.

DVR methods have been pioneered in recent years by the Light *et al.*,[12-14] primarily for use in vibrational eigenvalue problems, and Colbert and Miller[16] have recently shown that DVR provides an efficient L^2 basis set for reactive scattering calculations via the S-matrix Kohn variational method. The two major advantages of a DVR over a conventional basis set representation are that no integrals are required in order to construct the Hamiltonian matrix, and that the latter is an extremely sparse matrix so that the resulting linear algebra calculations (i.e., diagonalization or inversion) is considerably simplified. In this work we utilize the DVR of Colbert *et al.*,[16] which is especially simple and easy to use, in order to construct a grid point representation of Eq. (1.5).

The second key feature in our present approach, is the use of absorbing boundary conditions (ABC). Absorbing boundaries have been employed by a number of workers,[17-21] mostly by those carrying out time-dependent wave packet calculations on a coordinate grid. ABC prevent parts of the wave packet that reach the edge of the grid from unphysical reflection back toward the interaction region. This is accomplished by introducing an imaginary part to the potential-energy function,

$$V(\mathbf{q})\rightarrow V(\mathbf{q})-i\Gamma(\mathbf{q})/2, \tag{1.6}$$

where $\mathbf{q}\equiv\{q_i,\ i=1,...,F\}$ are the coordinates of the system. $\Gamma(\mathbf{q})$ is essentially zero in the physically relevant region of space, and is positive at the edge of the coordinate grid in order to absorb flux that reaches this region of space.

ABC can be thought of as a modified version of the formal convergence factor used in defining the Green's function in Eq. (1.5b), which can also be represented in terms of the time evolution operator,[22]

$$G(E^+)=\lim_{\epsilon\rightarrow 0}(E+i\epsilon-H)^{-1}$$
$$=\lim_{\epsilon\rightarrow 0}(i\hbar)^{-1}\int_0^\infty dt e^{i(E+i\epsilon-H)t/\hbar}. \tag{1.7}$$

Finite ϵ in Eq. (1.7) provides a factor $\exp(-\epsilon t/\hbar)$ in the integrand which assures convergence of the time integral. Another limiting form would be to introduce a time cutoff,

$$G(E^+)=\lim_{\tau\rightarrow\infty}(i\hbar)^{-1}\int_0^\tau dt e^{i(E-H)t/\hbar}, \tag{1.8a}$$

which can be thought of as Eq. (1.7) with a time-dependent ϵ,

$$\epsilon(t)=\begin{cases}0, & t<\tau\\ \infty, & t>\tau.\end{cases} \tag{1.8b}$$

One immediately sees the formal equivalence of adding a *negative* imaginary part to the potential energy [Eq. (1.6)], to adding a *positive* imaginary part to the energy E [Eq. (1.7)], i.e.,

$$\epsilon\leftrightarrow\Gamma/2, \tag{1.9}$$

provided that one allows ϵ to be a function of coordinates. The time-dependent ϵ of Eq. (1.8b) also suggests that ϵ should be chosen to be essentially zero in the interaction region (i.e., short time) and positive at the edge of the physically relevant region of space (i.e., long time).

Section II first summarizes the DVR and ABC methodologies as we use them to evaluate the cumulative reaction probabilities via Eq. (1.5). The results of test calculations are given in Sec. III, first for a one-dimensional (1D) barrier problem and then for the collinear $H+H_2\rightarrow H_2+H$ reaction. It is very encouraging that the number of "basis functions", i.e., DVR grid points needed to achieve convergence for $N(E)$ is about a factor of 4 less than the number needed to achieve convergence in earlier reactive scattering calculations for the S-matrix itself.[16] Thus, not only does the present "direct" approach require no reference to asymptotic (reactant or product) information, but the region of the potential-energy surface needed to determine the cumulative reaction probability is considerably smaller than that necessary to determine the state-to-state scattering information (i.e., the S matrix). Thus, the hope that a "direct" calculation of $N(E)$ will be considerably simpler than a full state-to-state reactive scattering calculation seems to be realizable.

II. METHODOLOGY

A. The discrete variable representation

We consider an F-dimensional Cartesian Hamiltonian

$$H=\sum_{\alpha=1}^{F}\frac{-\hbar^2}{2m_\alpha}\frac{d^2}{dq_\alpha^2}+V(\mathbf{q}), \tag{2.1}$$

and introduce an equally spaced grid for each coordinate q_α,

$$q_\alpha^{j_\alpha}=j_\alpha\Delta q_\alpha,$$
$$j_\alpha=0,\pm 1\pm 2,..., \tag{2.2}$$

where Δq_α is the grid spacing and $\alpha=1,...,F$. The potential-energy matrix is diagonal, as in all DVR methods,[12-16]

$$V_{j_1,...,j_F j_1',...,j_F'}=\delta_{j_1 j_1'}\cdots\delta_{j_F j_F'}V(q_1^{j_1},...,q_F^{j_F})$$
$$=V(\mathbf{q}_j)\prod_{\alpha=1}^{F}\delta_{j_\alpha j_\alpha'}, \tag{2.3a}$$

and the kinetic energy is a sum of one-dimensional matrices

$$T_{j_1,\ldots,j_F j'_1,\ldots,j'_F} = \sum_{\alpha=1}^{F} T^{\alpha}_{j_\alpha j'_\alpha} \prod_{\beta=1,\beta\neq\alpha}^{F} \delta_{j_\beta j'_\beta}, \tag{2.3b}$$

each of which is given by[16]

$$T^{\alpha}_{jj'} = \frac{\hbar^2}{2m_\alpha \Delta q_\alpha^2} (-1)^{j-j'} \begin{cases} \pi^2/3 & j=j' \\ 2/(j-j')^2 & j\neq j'. \end{cases} \tag{2.3c}$$

The Hamiltonian matrix $H_{j_1,\ldots,j_F j'_1,\ldots,j'_F}$ is thus very easy to construct and is extremely sparse.

The infinite grid defined by Eq. (2.2) is next adapted to the shape of the potential surface by using an energy cutoff criterion,[13(a),16] i.e., only grid points for which

$$V(\mathbf{q}) < V_c \tag{2.4}$$

are retained, where V_c is the cutoff value of the potential energy. Since the points that are discarded are in a classically forbidden regime for states with energies lower than V_c, the grid generated by Eq. (2.4) will provide an accurate description of all states with energies sufficiently below V_c. The energy cutoff provides a very simple way of generating points that follow the shape of a given potential-energy surface, and convergence is easily checked by increasing the value of V_c.

The flux operator F is defined in terms of a surface in coordinate space that separates reactants from products. It is specified most generally by equating some function of coordinates to zero,

$$f(\mathbf{q}) = 0. \tag{2.5a}$$

A simple example of this is

$$f(\mathbf{q}) = q_F, \tag{2.5b}$$

i.e., the $F-1$ dimensional surface on which the reaction coordinate q_F is constant (here zero). The flux operator is then given by

$$F = \frac{i}{\hbar}\{H, h[f(\mathbf{q})]\}, \tag{2.6a}$$

where H is the total Hamiltonian and h is the Heaviside function

$$h(\xi) = \begin{cases} 1, & \xi > 0 \\ 0, & \xi < 0. \end{cases} \tag{2.6b}$$

[One recognizes Eq. (2.5a) as the Heisenberg time derivative, $F = (d/dt)h(f)$.] Since $h[f(\mathbf{q})]$ is a function of coordinates, the potential-energy part of H commutes with it, so that Eq. (2.6a) becomes

$$F = \frac{i}{\hbar}[T, h(f)]. \tag{2.6c}$$

For the simple choice of $f(\mathbf{q})$ in Eq. (2.5b), Eq. (2.6c) reduces to

$$F = \frac{1}{2}\left[\frac{p_F}{m}\delta(q_F) + \delta(q_F)\frac{p_F}{m}\right], \tag{2.6d}$$

a form that has been used in most calculations to date for the reactive flux.[2(b)-11]

However, rather than using Eq. (2.6d) for the flux operator, in this paper we utilize Eq. (2.6c). Not only is it more general, but we have also found it to give more rapid convergence in terms of grid size. The DVR for the flux operator, Eq. (2.6c) is thus

$$F_{\mathbf{j},\mathbf{j}'} = \frac{i}{\hbar} T_{\mathbf{j},\mathbf{j}'}\{h[f(\mathbf{q}_\mathbf{j})] - h[f(\mathbf{q}_{\mathbf{j}'})]\}, \tag{2.7}$$

showing explicitly that in addition to the grid point representation of the kinetic energy—which is already at hand from construction of the Hamiltonian—one only needs to evaluate the function $f(\mathbf{q})$ at the various grid points to see if $f>0$ or <0. Equation (2.7) shows that the flux matrix element is nonzero only if the grid points $\mathbf{q}_{\mathbf{j}'}$ and $\mathbf{q}_\mathbf{j}$ are on opposite sides of the dividing surface.

The version of the DVR for the flux operator based on Eq. (2.6d) is given in Appendix A.

B. Absorbing boundary conditions

As discussed in Sec. I regarding Eqs. (1.6)–(1.9), a function $\epsilon(\mathbf{q}) \equiv \Gamma(\mathbf{q})/2$ is introduced which is essentially zero in the physically relevant interaction region and turns on at the edge of the DVR grid. Since $-i\epsilon(\mathbf{q})$ is a potential-energy-like term, its DVR is diagonal and simply added to the potential matrix of Eq. (2.3a).

We first consider the form of the absorbing potential in the one-dimensional case

$$\epsilon(\mathbf{q}) = \epsilon(q), \tag{2.8}$$

where $q=0$ is the transition state (and location of the dividing "surface"). Denoting by $q_{\max}$ the grid truncation point, we consider (i) a power law turn on

$$\epsilon(q) = \begin{cases} \lambda[(q-q_0)/(q_{\max}-q_0)]^n & q \geqslant q_0 \\ 0 & 0 < q < q_0, \end{cases} \tag{2.9a}$$

and (ii) a Woods–Saxon potential

$$\epsilon(q) = \frac{2\lambda}{1+\exp[(q_{\max}-q)/\eta]}, \quad 0<q. \tag{2.9b}$$

A similar function is placed to the left of the interaction region ($q<0$) in both cases.

The conditions and limitations on $\epsilon(q)$ are that one wants it to turn on sufficiently rapidly to absorb the flux over as short a distance as possible, but not to turn on sharply enough to cause reflection back toward the physically relevant region of space. These aspects were clearly discussed by Neuhauser and Baer[21(a)] for the case of a linear absorbing potential, i.e., $n=1$ in Eq. (2.9a). Appendix B presents a discussion of these issues based on a semiclassical (WKB) treatment. $\epsilon(q)$ is plotted in Fig. 1 for several choices of the parameters to be employed in the following calculations. Physical intuition leads us to expect the second family of curves [Eq. (2.9b)] to better serve our purpose. The latter allows the low translational energy components, which suffer more from reflection, to encounter a shallow enough slope without forcing the magnitude of the absorbing potential to be unduly small. The quadratic curve of Fig. 1 is clearly an intermediate case between the constant [$n=1$ in Eq. (2.9a)] and the exponential one [Eq. (2.9b)]. These expectations are borne out in Sec. III.

For a multidimensional system it is convenient to take $\epsilon(\mathbf{q})$ as some one-dimensional function in Eq. (2.9),

$$\epsilon(\mathbf{q}) = \epsilon[Q(\mathbf{q})], \tag{2.10}$$

where $Q(\mathbf{q})$ is some function of all the coordinates $\mathbf{q}$. The functional form of $\epsilon(Q)$ determines how the absorbing potential turns on upon entering the absorbing region as for the 1D case, and the choice of $Q(\mathbf{q})$ determines the location of the "absorbing strip" which surrounds (and defines) the interaction region. Examples of this are discussed more explicitly with regard to the application in Sec. III B.

C. Summary of methodology

The DVR grid points are laid down according to Eq. (2.2) and then truncated by the energy cutoff criterion, Eq. (2.4). An absorbing potential, Eqs. (2.9)–(2.10), surrounds (and defines) the interaction region. The DVR matrices of the kinetic $\mathbf{T}$ and potential $\mathbf{V}$ energies are given by Eq. (2.3) (the matrix $\boldsymbol{\epsilon}$ is also a diagonal potential-energy-like matrix) and the DVR, or grid point representation for the Green's function, is thus

$$\mathbf{G}(E^+) = (E\mathbf{I} - \mathbf{T} - \mathbf{V} + i\boldsymbol{\epsilon})^{-1}. \tag{2.11}$$

The DVR matrix for the flux operator is given by Eq. (2.7), so that Eq. (1.5) for the cumulative reaction probability becomes

$$\begin{aligned} N(E) &= 2\hbar^2 \mathrm{tr}(\mathbf{F}\cdot \mathrm{Im}\,\mathbf{G}\cdot\mathbf{F}\cdot \mathrm{Im}\,\mathbf{G}) \\ &= \hbar^2 \mathscr{D}\,[\mathrm{tr}(\mathbf{F}\cdot\mathbf{G}\cdot\mathbf{F}\cdot\mathbf{G}^*) - \mathrm{tr}(\mathbf{F}\cdot\mathbf{G}\cdot\mathbf{F}\cdot\mathbf{G})], \end{aligned} \tag{2.12}$$

where $\mathbf{G} \equiv \mathbf{G}(E^+)$.

Note added in proof. We have recently been able to show that the basic equation for $N(E)$, Eq. (2.12), can be cast in the following equivalent but simpler and more useful form:

$$N(E) = \mathrm{tr}(\boldsymbol{\Gamma}_r\cdot\mathbf{G}\cdot\boldsymbol{\Gamma}_p\cdot\mathbf{G}^*), \tag{2.13a}$$

where $\mathbf{G}$ is given by Eq. (2.11) (with $\epsilon \equiv \Gamma/2$), and Γ_r (Γ_p) is the absorbing potential in the reactant (product) region; since these regions do not overlap, $\Gamma = \Gamma_r + \Gamma_p$. Because the absorbing potentials are diagonal in the DVR, this result can be also written as

$$N(E) = \sum_{\mathbf{j},\mathbf{j}'} \Gamma_r(\mathbf{q}_\mathbf{j}) |G_{\mathbf{j},\mathbf{j}'}|^2 \Gamma_p(\mathbf{q}_{\mathbf{j}'}), \tag{2.13b}$$

which shows that only matrix elements of the Green's operator between points $\mathbf{q}_\mathbf{j}$ in the reactant absorbing strip and $\mathbf{q}_{\mathbf{j}'}$ in the product absorbing strip are needed. Equation (2.13) also shows explicitly that $N(E)$ does not depend on the choice of the dividing surface [cf. Eq. (2.5) *et seq.*], so long as it lies between the reactant and product absorbing strips. Calculations of $N(E)$ for reactions in 3D space are being carried out using these expressions and will be reported in our next paper on this subject.

III. RESULTS AND DISCUSSION

A. One-dimensional results

It is useful to illustrate the convergence properties of the method described in Sec. II by first considering a 1D, analytically soluble model problem. In this subsection we present our results for the Eckart barrier

$$V(q) = V_0 \mathrm{sech}^2(q/a) \tag{3.1}$$

(see Fig. 1). The barrier height $V_0 = 0.425$ eV and the mass

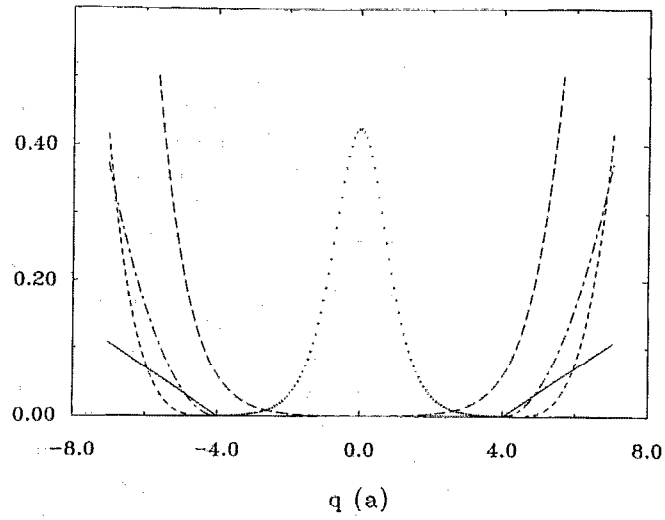

FIG. 1. (···) The Eckart potential [Eq. (3.1)] with $V_0 = 0.425$ eV. (—) Linear absorbing potential [$n = 1$ in Eq. (2.9a)] with $\lambda = 0.11$ eV. (–·–·–·) Quadratic absorbing potential [$n = 2$ in Eq. (2.9a)] with $\lambda = 0.38$ eV. (---) Quartic absorbing potential [$n = 4$ in Eq. (2.9a)] with $\lambda = 0.44$ eV. (— — —) Woods–Saxon absorbing potential [Eq. (2.9b)] with $\eta = 0.8a$ and $\lambda = 1.1$ eV.

$m = 1060$ a.u. are chosen to correspond approximately to the $H + H_2$ collision. For generality we measure distances in units of a.

Figure 2 illustrates the reaction probability, $N(E)$, using the Woods–Saxon form [Eq. (2.9b)] with various values of η for the absorbing potential. The solid curve shows the exact probability[23]

$$N^{\mathrm{exact}}(E) = \{1 + [\cosh(c)/\sinh(b)]^2\}^{-1}, \tag{3.2}$$

with

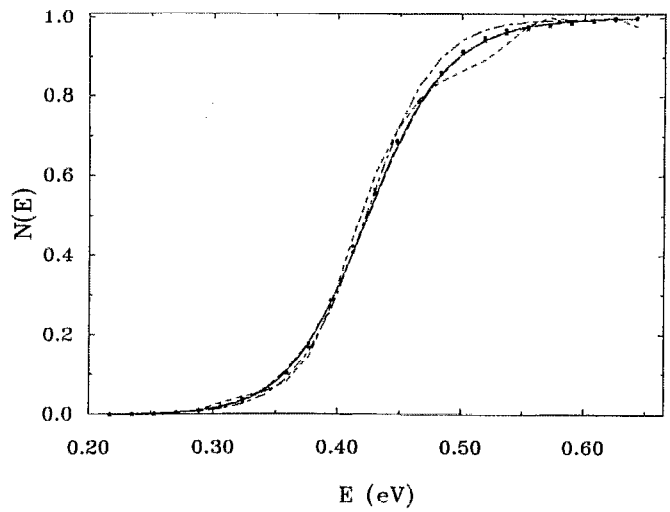

FIG. 2. Reaction probability $N(E)$ for the Eckart barrier using the Woods–Saxon form for the absorbing potential, with $q_{\max} = 4.5a$: (—) Exact result [Eq. (3.2)]; (–·–·–·) $\eta = 0.15a$; (○) $\eta = 0.30a$; (— — —) $\eta = 0.50a$; (*) $\eta = 0.80a$; (---) $\eta = 1.10a$.

$$b = a\pi(2mE/\hbar^2)^{1/2},$$

$$c = (\pi/2)\left[(8V_0ma^2/\hbar^2) - 1\right]^{1/2}.$$

As shown in Fig. 2, the results are insensitive to the value of η over a wide range, $0.3a \leqslant \eta \leqslant 0.8a$, throughout the entire energy regime. Nevertheless, with too small a choice of η (the dotted-dashed curve in Fig. 2), the absorbing potential becomes steep enough to cause reflection, while with a very large η (the dashed curve of Fig. 2) $\epsilon(q)$ penetrates the interaction region and interferes with the dynamics.

Figure 3 shows the reaction probability obtained using a linear absorbing potential [$n = 1$ in Eq. (2.9a)] with several choices of q_0. Again, the exact curve is reproduced (to within 0.5%) using a range of q_0 values, $1a \leqslant q_0 \leqslant 4a$. When q_0 is increased beyond this range, the absorbing region allows some transmission (see Appendix B), while with too small a value of q_0 the imaginary potential is switched on early enough to deteriorate the reaction dynamics. It should be noted that a much larger grid is needed with the linear form (Fig. 3) as compared to that required with the Woods–Saxon potential (Fig. 2), in order to exhibit comparable insensitivity to the parameters of $\epsilon(q)$.

Although accurate results can be obtained with widely different forms of the absorbing potential, the convergence properties of the method with respect to the grid size are clearly dependent on the form of $\epsilon(q)$. As pointed out in Sec. II, for the present study it is of particular importance to minimize the size of the grid, not only for practical reasons, but also since the physical information required to compute the flux correlation expressions is expected to concentrate in a relatively small region, centered about the dividing surface.

In Fig. 4 we plot the percent error

$$\frac{N^{\text{exact}}(E) - N^{\text{numerical}}(E)}{N^{\text{exact}}(E)} \times 100$$

vs the grid dimension ($q_{\max}$) using Eq. (2.9a) for $\epsilon(q)$ with $n = 1$, 2, and 4. The (constant) energy is $E = 0.32$ eV and the value of λ is chosen in each case so as to optimize the convergence rate. The corresponding absorbing potentials are shown in Fig. 1. As may be expected from Fig. 1, a broader absorbing region is needed to totally absorb the flux in the case of a linear form, as compared to that required using a quadratic function. The quartic form leads to poorer convergence, again a result which may be qualitatively anticipated from Fig. 1.

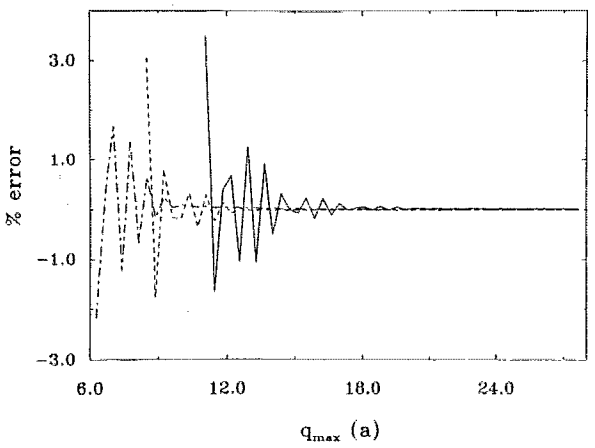

FIG. 4. Percent error in $N(E)$ vs $q_{\max}$ at $E = 0.32$ eV, using Eq. (2.9a) for $\epsilon(q)$: (—) $n = 1$; (-·-·-·) $n = 2$; (---) $n = 4$. The values of λ and q_0 in each case are as in the corresponding curve of Fig. 1.

Figure 5 shows the percent error as a function of the grid dimension using the Woods–Saxon form for $\epsilon(q)$. The corresponding absorbing potential is shown as a dashed curve in Fig. 1. The three curves of Fig. 5 correspond to three different energies: $E = 0.32$ eV, which is in the deep tunneling regime, $E = V_0 \approx 0.425$ eV, and $E = 0.76$ eV, well above the reaction barrier. As the energy is increased, the system becomes more classical-like and less sensitive to the details of

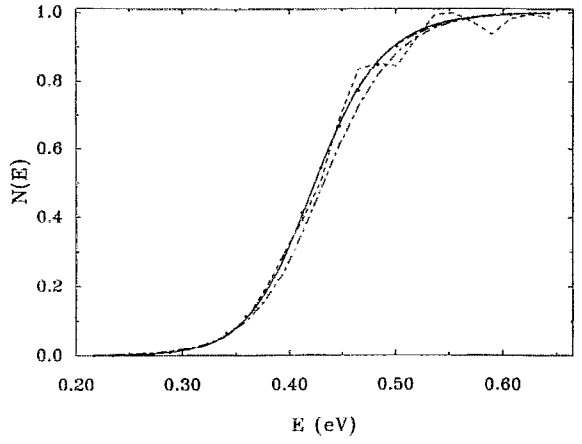

FIG. 3. Reaction probability for the Eckart barrier using a linear absorbing potential, with $q_{\max} = 8.0a$: (—) Exact result [Eq. (3.2)]; (-·-·-·) $q_0 = 0.1a$; (○) $q_0 = 1.0a$; (— — —) $q_0 = 4.0a$; (---) $q_0 = 6.5a$.

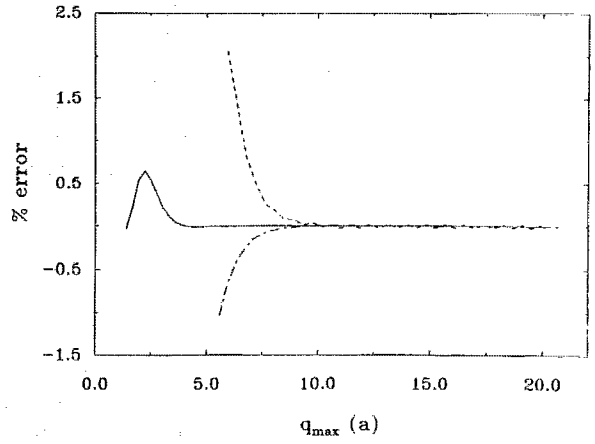

FIG. 5. Percent error in $N(E)$ vs $q_{\max}$ using the Woods–Saxon form for $\epsilon(q)$: (—) $E = 0.76$ eV; (-·-·-·) $E = V_0 \approx 0.425$ eV; (---) $E = 0.32$ eV. The corresponding $\epsilon(q)$ is shown as a dashed curve in Fig. 1.

the potential away from the saddle point. Consequently, the convergence rate improves rapidly. The low-energy curve of Fig. 5 compares favorably with the three curves of Fig. 4, in accord with our qualitative expectations based on Fig. 1.

In Fig. 6 we examine the convergence rate of $N(E)$ with respect to the *density* of grid points. Plotted is the percent error at several energies vs the number of grid points per deBroglie wavelength, $N_B = 2\pi/k\Delta_q$, where $k = (2mE/\hbar^2)^{1/2}$. The number of grid points per wave required to attain $\approx 0.1\%$ accuracy is of the order of $N_B \approx 2.5$–3.5 at all energies. At low and intermediate energies the results converge at a somewhat higher value ($N_B \approx 3.5$), while the more energetic collisions require roughly 2.5 points per full wave. At still higher energies, $E \gg V_0$, the value of N_B with which the results converge remains practically constant at 2.5.

B. The collinear H+H$_2$ reaction

The H + H_2 collision serves as a standard test application for new methods, the major reason being the availability of an accurate potential surface and benchmark calculations for this system. In this section we present and discuss the results of calculations using the method described in Sec. II for the collinear H + H_2 reaction using the LSTH potential surface.[24]

A natural choice of coordinates for the present method, which centers attention in the vicinity of the saddle point, are the normal-mode coordinates of the transition state. The doubly infinite DVR grid is thus laid in these coordinates (q_1,q_2), where q_2 corresponds to the asymmetric stretch (or reaction coordinate), and then truncated by the energy cutoff criterion, Eq. (2.4), and also by the location of the absorbing potential (see following). An obvious choice for the dividing "surface" for this symmetric system, is the $q_2 = 0$ line [i.e., $f(\mathbf{q}) = q_2$ in Eq. (2.5a)]. One thus obtains a DVR grid that follows the shape of the potential-energy surface and is localized about the dividing surface. Convergence can then be systematically checked by increasing the energy cutoff parameter V_c of Eq. (2.4) and by extending the region bounded by the absorbing potential.

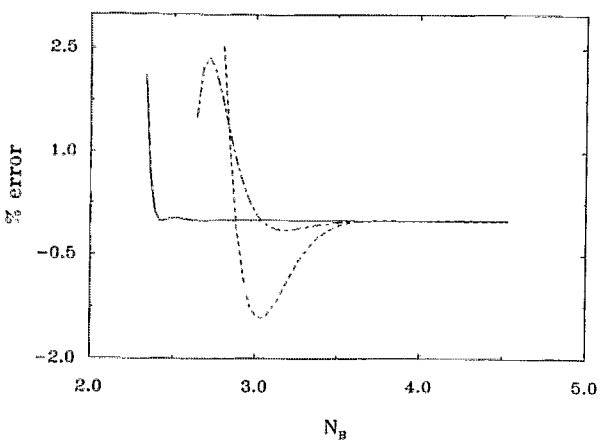

FIG. 6. Percent error in $N(E)$ as a function of the number of grid points per deBroglie wavelength N_B. $\epsilon(q)$ is of the Woods–Saxon form with $\eta = 0.8a$ and $\lambda = 1.1$ eV: (—) $E = 0.76$ eV; (-·-·-·) $E = V_0 \approx 0.425$ eV; (---) $E = 0.32$ eV.

There are a variety of ways of choosing the location of the absorbing potential, i.e., choosing the function $Q(\mathbf{q}) \equiv Q(q_1,q_2)$ in Eq. (2.10). Figure 7 shows contour plots of the LSTH potential-energy surface with typical DVR grids superimposed on it. Figures 7(a)–7(c) show three different possibilities for the location of the absorbing potential; in all cases $\epsilon(\mathbf{q}) \equiv \epsilon(q_1,q_2)$ is essentially zero in the interior (interaction) region and turns on at the edge of the cross-hatched region, producing essentially complete absorption by the outer edge of the cross hatched region. In Fig. 7(a) the function Q is

$$Q(q_1,q_2) = \max[R_a(q_1,q_2),R_b(q_1,q_2)], \tag{3.3a}$$

where R_a and R_b are the reactant and product translational (Jacobi) coordinates, respectively. Figure 7(b) corresponds to choosing the absorbing potential to be a function of the *hyperspherical radius*,

$$Q(q_1,q_2) = [(q_1 - q_1^0)^2 + (q_2 - q_2^0)^2]^{1/2}, \tag{3.3b}$$

where (q_1^0,q_2^0) is the origin of the hyperspherical coordinate system. Finally, Fig. 7(c) corresponds to choosing $\epsilon(\mathbf{q})$ to be a function only of the Cartesian reaction coordinate q_2,

$$Q(q_1,q_2) = |q_2|. \tag{3.3c}$$

We have found that all three choices give correct results, but that the third choice, Eq. (3.3c), is the most efficient, i.e., leads to convergence with the smallest region and thus the fewest number of DVR grid points. The advantage of the configuration of Eq. (3.3c) [Fig. 7(c)] follows from the fact that the present approach allows us to focus attention on a relatively narrow strip along the dividing surface, without having to extend the grid into the reactant or product valleys.

For all calculations discussed in this subsection we have employed the Woods–Saxon form [Eq. (2.9b)] for the absorbing potential. Accurate results were also obtained using various powers in $q_2 - q_{2,0}$ [Eq. (2.9a)]. The grid required was larger however, particularly in the high-energy regime, where more than a single vibrational channel is open, and the requirements of complete absorption and no reflection need be satisfied at more than a single translational energy. This effect may be qualitatively rationalized by inspection of Fig. 1.

The cumulative H + H_2 reaction probability, as calculated via Eqs. (2.9b)–(2.12) and (3.3c), is plotted vs the total energy in Fig. 8, and compared with the R-matrix propagation results of Bondi *et al.*[25] The agreement is exact to within the degree of convergence of the results of Ref. 25 ($\lesssim 1\%$ at the low energies and up to 5% at the high-energy edge[25]).

Figure 9 examines more closely the behavior of the probability curve as the grid size is gradually reduced. Thus, with $q_2^{\max} = 3$ a.u. (corresponding to a total of 90 DVR points), the results have converged to better than 1% throughout the energy range examined. With $q_2^{\max} = 2$ a.u. [corresponding to the 64 grid points shown in Fig. 7(c)] the

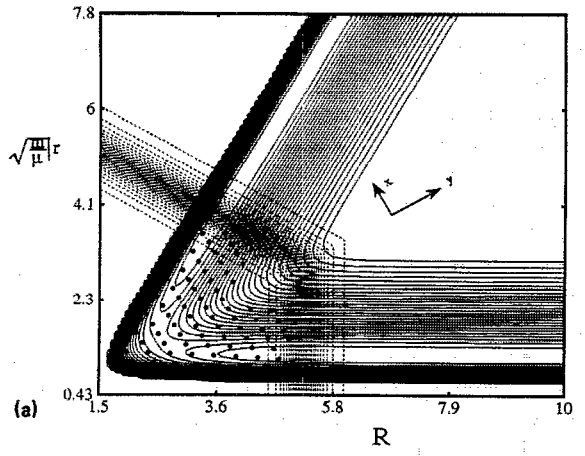

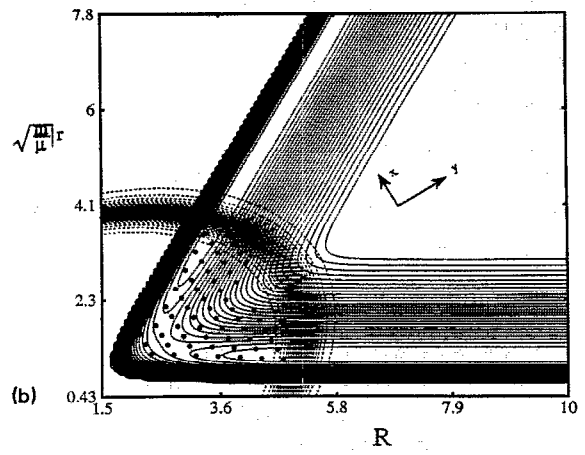

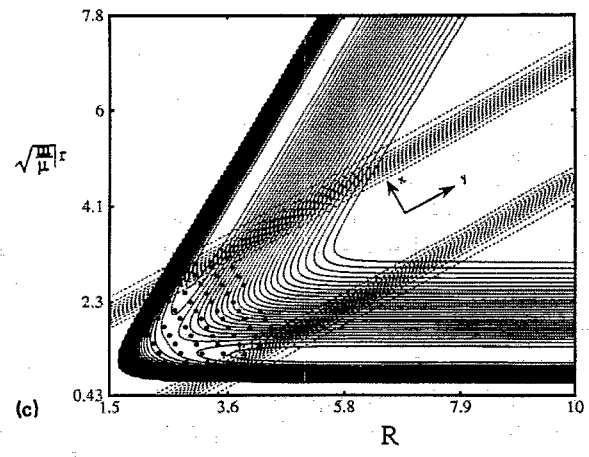

FIG. 7. The LSTH potential surface as a function of the mass weighted Jacobi coordinates $\{R,r\}$. q_1 and q_2 are the normal-mode coordinates of the transition state. The dashed contours show the absorbing potential $\epsilon[Q(q_1,q_2)]$ [Eq. (2.9b)]: (a) For $Q(q_1,q_2)$ of Eq. (3.3a); (b) for $Q(q_1,q_2)$ of Eq. (3.3b); (c) for $Q(q_1,q_2)$ of Eq. (3.3c). The distribution of grid points and the parameters of ϵ in Fig. 7(c) correspond to the calculation shown as a dashed curve in Fig. 9.

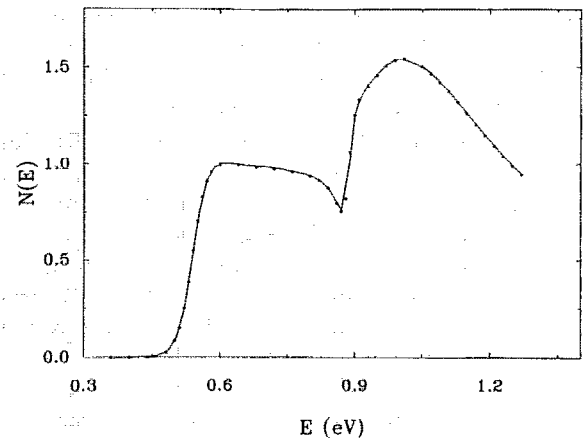

FIG. 8. Cumulative reaction probability for the collinear $H + H_2$ reaction: (●●●) R matrix propagation results (summed over internal states) (Ref. 25); (—) present results.

accuracy varies between 0.1% and 1.5%. Reasonable agreement with the exact curve at most energies is obtained with $q_2^{\max} = 1.8$ a.u. and as few as 45 grid points.

Finally, in Fig. 10, we illustrate the convergence rate of the cumulative probability as a function of the grid dimension, $q_2^{\max}$, and the energy cutoff parameter V_c. The percent error is computed with respect to the fully converged calculations of Zhang.[26] The total energy is $E = 0.9678$ eV, about 0.19 eV above the threshold of the second vibrational channel.

The results shown in Fig. 10 converge to 0.02% with $V_c = 5$ eV and to about 0.5% when the cutoff parameter is halved to 2.5 eV. The former accuracy corresponds to a total

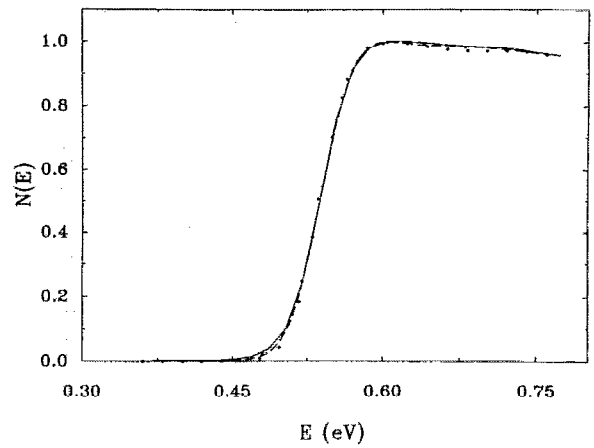

FIG. 9. Same as in Fig. 8 with different values of $q_2^{\max}$: (—) $q_2^{\max} = 3.0$ a.u. (corresponding to 90 DVR points); (---) $q_2^{\max} = 2.0$ a.u. (corresponding to the 64 DVR points shown in Fig. 7); (○) $q_2^{\max} = 1.8$ a.u. (corresponding to 45 DVR points).

of 202, and the latter to a total of 104 grid points. A larger grid is required in the multiopen channels energetic regime as compared to the low-energy range considered in Fig. 9. This effect is due to the presence of the low translational energy ($E_{v=1}^{\text{trans}} \approx 0.19$ eV) component. The latter requires that the slope of the absorbing potential be kept relatively small so as to avoid reflection. In order to completely absorb the high translational energy component the width of the absorbing region is then required to be larger (see Appendix B). Nevertheless, the total number of grid points required to attain $\approx 0.5\%$ convergence in this less favorable energetic regime is encouragingly small.

IV. CONCLUDING REMARKS

The use of a discrete variable representation and absorbing boundary conditions provides a very convenient way of calculating the outgoing wave Green's function $\mathbf{G}(E^+) \equiv (E\mathbf{I} - \mathbf{H} + i\epsilon)^{-1}$. The primary advantage of this methodology over earlier variational basis set approximations[27] for $G(E^+)$ is that the present approach does not require any explicit information about the asymptotic channel states. The variational methods require that one includes basis functions that explicitly contain outgoing radial waves in each asymptotic open channel, while the ABC avoids this by absorbing all outgoing flux *en route* to the asymptotic region. The absorbing potential, $\epsilon(\mathbf{q})$, may be thought of as a generalization of the formal convergence parameter introduced in defining $G(E^+)$ [Eq. (1.5b)]. Allowing ϵ to be a potential-energy-type operator thus provides much more flexibility in obtaining an efficient approximation for $G(E^+)$; by having $\epsilon(\mathbf{q})$ essentially zero in the physically relevant region of space, and nonzero only at the edges to absorb outgoing flux, one does not need to take the $\epsilon \to 0$ limit as when ϵ is a constant. [The approximation we obtain for $G(E^+)$, however, is only valid for computing matrix elements $\langle \Phi_2 | G(E^+) | \Phi_1 \rangle$ for states Φ_1 and Φ_2 localized to the interaction region.]

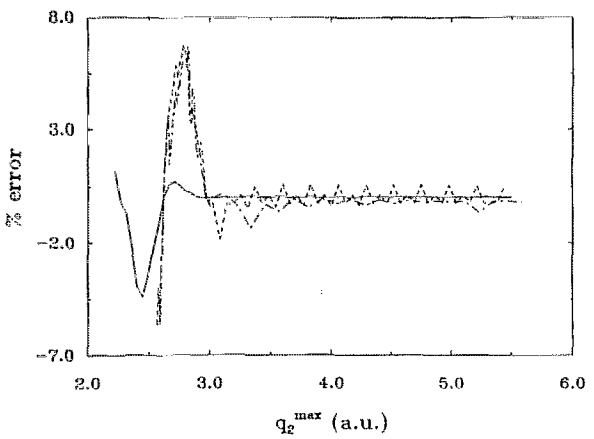

FIG. 10. Percent error in the $H + H_2$ cumulative probability at $E = 0.9678$ eV, as a function of $q_2^{\max}$: (—) $V_c = 5.0$ eV; (---) $V_c = 3.0$ eV; (-·-·-·) $V_c = 2.5$ eV.

Having $G(E^+)$ available thus provides the microcanonical density operator $\delta(E-H)$, Eq. (1.5b), so that the flux–flux expression for the cumulative reaction probability, Eq. (1.5a), can be readily evaluated. The results presented in Sec. III B for the benchmark reaction $H + H_2 \to H_2 + H$ are quite impressive. One achieves convergence for the cumulative reaction probability with roughly one-quarter of the number of grid points needed to determine the state-to-state scattering (i.e., the S matrix).[16] This is the "hoped for" efficiency of a "direct" calculation of the cumulative reaction probability provided by the flux–flux formalism.[1,2]

Finally, as an aside, we note that the DVR–ABC representation of $G(E^+)$ also provides the possibility of complete state-to-state scattering calculations, i.e., the reactive scattering matrix. Thus, let Φ_i and Φ_f be any distorted incoming waves for states i and f, with asymptotic boundary conditions

$$\Phi_i(\mathbf{r},R) \sim \sum_j \phi_j(\mathbf{r}) v_j^{-1/2} (-e^{-ik_jR}\delta_{j,i} + e^{ik_jR} S_{j,i}^0), \tag{4.1}$$

and similar for Φ_f. Here R denotes the asymptotic (Jacobi) translational coordinate and $\mathbf{r}$ all the remaining internal coordinates. For clarity of notation we omitted the arrangement channel indices (which differ for states Φ_i and Φ_f in the case of a reactive collision). A formally exact expression for the S matrix is

$$S_{f,i} = S_{f,i}^0 + \frac{i}{\hbar} [\langle \Phi_f | H - E | \Phi_i \rangle + \langle \chi_f | G(E^+) | \chi_i \rangle], \tag{4.2}$$

where

$$\chi_i = (H - E)\Phi_i, \tag{4.3a}$$

$$\chi_f = (H - E)\Phi_f. \tag{4.3b}$$

The distorted waves Φ_i, Φ_f can be anything, from free (i.e., undistorted) waves

$$\Phi_i(\mathbf{r},R) = \phi_i(\mathbf{r}) v_i^{-1/2} (-e^{-ik_iR} + e^{ik_iR}), \tag{4.4a}$$

with

$$S_{j,i}^0 = \delta_{j,i}, \tag{4.4b}$$

to the exact solution of the Schrödinger equation Ψ_i and Ψ_f with the boundary conditions of Eq. (4.4), in which case $S_{j,i}^0 = S_{j,i}$, the exact S matrix. In all cases the functions χ_i and χ_f of Eqs. (4.3) are L^2 functions localized to the interaction region; they will be smaller, and presumably localized to closer in regions, the more accurately Φ_i and Φ_f approximate the exact wave functions Ψ_i and Ψ_f. It is thus clear how one proceedes. The DVR–ABC approximation for $G(E^+)$ is used in Eq. (4.2). For the two-dimensional example treated in Sec. III B, the explicit expression for the last term in Eq. (4.2) is

$$\langle \chi_f | G(E^+) | \chi_i \rangle = \mathbf{M}_f^T \cdot \mathbf{G} \cdot \mathbf{M}_i, \tag{4.5}$$

where $\mathbf{G}$ is the DVR–ABC Green's function of Eq. (2.11), and

$$(\mathbf{M}_i)_{j_1 j_2} = \sqrt{\Delta q_1 \Delta q_2}\,\langle q_1^{j_1}, q_2^{j_2}|H - E\,|\Phi_i\rangle; \tag{4.6}$$

i.e., one lets $(H-E)$ operate on Φ_i and then evaluates this at the grid point $(q_1^{j_1}, q_2^{j_2})$. A similar expression holds for $\mathbf{M}_f$.

The reader familiar with the S-matrix Kohn variational method will realize that the aforementioned approximation has many features in common with it, so it is not at all clear that the aforementioned procedure has any advantages over it for computing the complete S matrix. It may, however, bear further thought and investigation. The primary point of *this* paper is that the DVR–ABC approximation to $G(E^+)$ provides an efficient "direct" avenue to the cumulative reaction probability, and thus the rate constant, that avoids the necessity of a complete state-to-state calculation.

ACKNOWLEDGMENTS

We would like to thank Dr. J. N. L. Connor for sending us the numerical values of the reaction probabilities reported in Ref. 25. This work was supported by the Director, Office of Energy Research, Office of Basic Energy Sciences, Chemical Sciences Division of the U.S. Department of Energy under Contact No. DE-AC03-76SF00098. T.S. is supported by the National Science Foundation, Grant No. CHE-8920690.

APPENDIX A: ALTERNATIVE DVR FOR THE FLUX OPERATOR

We derive an alternative DVR for the flux operator, based on the special case of Eqs. (2.5b) and (2.6d). While the form suggested in the text [Eqs. (2.7)] has the formal advantage that it is manifestly independent of the coordinates, and the computational advantage that its matrix elements decay as $(j-j')^2$ away from the diagonal [compare Eqs. (A5)–(A9)], the form derived later is mathematically transparent and suggestive of the suitability of the grid representation for flux correlation expressions.

Following the standard DVR procedure,[12–15] we first choose an appropriate finite-basis representation (FBR) for F $\{\psi_n, n=0,\ldots,N-1\}$, guided by the existence of a quadrature rule for evaluation of the potential matrix elements. Specifically, we choose a particle-in-a-box basis

$$\psi_n(q_F) = \sqrt{1/b}\,\sin\left(\frac{n\pi}{2b}\,(q_F+b)\right) \tag{A1a}$$

(b denoting the box size), and place grid points at the nodes of ψ_N,

$$q_F^j = j\Delta q, \quad \Delta q = 2b/N. \tag{A1b}$$

In Eqs. (A1) we focused on the symmetric interval case $(-b \leqslant q_F \leqslant b)$ appropriate for a reaction-type coordinate.

Thus

$$\mathbf{V}^{\mathrm{FBR}} = \mathbf{U}\mathbf{V}^{\mathrm{DVR}}\mathbf{U}^T, \tag{A2}$$

where $V^{\mathrm{DVR}}_{jj'} = V(q_F^j)\delta_{jj'}$, $U_{nj} = \sqrt{w}\psi_n(q_F^j)$, and we approximated $V^{\mathrm{FBR}}_{n,n'}$ by a Gauss Chebyshev quadrature of the second kind[15] with evenly spaced quadrature points $\{q_F^j\}$ [Eq. (A1b)] and constant weights $w_j = w = \Delta q$. Evidentially, this procedure becomes exact in the limit of large N.

The DVR of the flux operator can now be written as

$$\mathbf{F}^{\mathrm{DVR}} = \mathbf{U}^T\mathbf{F}^{\mathrm{FBR}}\mathbf{U}, \tag{A3}$$

where $\mathbf{F}^{\mathrm{FBR}}$ is the basis set representation of Eq. (2.6d),

$$F^{\mathrm{FBR}}_{n,n'} = \frac{\hbar}{2im}\left[\psi_n(0)\psi'_{n'}(0) - \psi'_n(0)\psi_{n'}(0)\right]. \tag{A4}$$

Using Eqs. (A1) and (A4) in Eq. (A3) we find

$$\mathbf{F}^{\mathrm{DVR}} = \frac{\Delta q\hbar}{2im}\,(\cdot\mathbf{v}\mathbf{d}\cdot - \cdot\mathbf{d}\mathbf{v}\cdot), \tag{A5}$$

where

$$\begin{aligned} v_j &\equiv v_j(0) \\ &= \delta(q_F^j) \\ &= \sum_n^{N-1} \psi_n(q_F^j)\psi_n(0) \\ &= \frac{1}{b}\sum_{n=1,3,\ldots}^{N-1} \cos\left(\frac{n\pi j}{N}\right) \\ &= \frac{1}{b}\sum_{k=0}^{N/2-1} \cos\left(\frac{2k\pi j}{N} + \frac{\pi j}{N}\right) \end{aligned} \tag{A6}$$

and

$$\begin{aligned} d_j &\equiv d_j(0) \\ &= \delta'(q_F^j) \\ &= \sum_n^{N-1} \psi_n(q_F^j)\psi'_n(0) \\ &= \frac{1}{b}\sum_{n=2,4,\ldots}^{N-1} \frac{n\pi}{2b}\sin\left(\frac{n\pi j}{N}\right) \\ &= \frac{1}{b}\sum_{k=1}^{(N-1)/2} \frac{k\pi}{b}\sin\left(\frac{2k\pi j}{N}\right). \end{aligned} \tag{A7}$$

The $v_j(q)$ form a grid representation for the coordinate operator, and the $(\hbar/im)d_j(q)$ form a grid representation for the velocity. Equation (A5) is thus a direct DVR transcription of Eq. (2.6d).

Summing Eqs. (A6) and (A7) over k [Ref. (28), Eqs. (1.342.1), (1.342.2), and (1.352.1)] we find

$$v_j = \delta_{j,0}\Delta q^{-1} \tag{A8}$$

and

$$\begin{aligned} d_j &= (1-\delta_{j,0})\,\frac{\pi}{b^2}\left[4\sin^2\left(\frac{\pi j}{N}\right)\right]^{-1} \\ &\quad\times\left[\sin\left(\frac{N+1}{N}\pi j\right)\Big/\sin\left(\frac{\pi j}{N}\right) - (N+1)(-1)^j\right] \\ &\overset{N\to\infty}{\to} -(1-\delta_{j,0})\Delta q^{-2}\,\frac{(-1)^j}{j}. \end{aligned} \tag{A9}$$

Equation (2.3c) in the text may be derived similarly, by transforming the basis set representation of the kinetic-energy operator,

$$T^{\mathrm{FBR}}_{n,n'} = \delta_{n,n'}\,\frac{\hbar^2}{2m}\left(\frac{n\pi}{2b}\right)^2,$$

using the analogous relation to Eq. (A3).

APPENDIX B: WKB DESCRIPTION OF THE REFLECTION AND TRANSMISSION BY AN ABSORBING POTENTIAL

We consider a one-dimensional system in a region where the actual (real) potential $V(q)$ is zero. The net effective potential $V(q) - i\epsilon(q)$ is thus the (imaginary) absorbing potential alone, i.e.,

$$V_{\text{eff}}(q) \equiv V(q) - i\epsilon(q) = -i\epsilon(q), \tag{B1}$$

and we assume the power law form of Eq. (2.9a) for $\epsilon(q)$

$$\epsilon(q) = \begin{cases} 0, & q < q_0 \\ \lambda\left(\dfrac{q - q_0}{q_{\max} - q_0}\right)^n, & q \geqslant q_0. \end{cases} \tag{B2}$$

The WKB approximation for the probability that a particle incident from the left, $q_{\text{initial}} \equiv q_1 < q_0$, and moving to the right ($+q$ direction) is reflected back to position $q_1 < q_0$, i.e., the *reflection probability* R, is given by

$$R = \left|\exp\left(2i\int_{q_1}^{q_t} dq k(q)\right)\right|^2 = \exp\left(-4\,\text{Im}\int_{q_0}^{q_t} dq k(q)\right), \tag{B3}$$

where $k(q)$ is the (complex) local momentum (in units of $\hbar$)

$$k(q) = \left(\frac{2m}{\hbar^2}\left[E - V_{\text{eff}}(q)\right]\right)^{1/2}, \tag{B4a}$$

and q_t is the (complex) turning point

$$k(q_t) = 0. \tag{B4b}$$

In light of Eq. (B1), $k(q)$ is given by

$$k(q) = k\left[1 + i\epsilon(q)/E\right]^{1/2}, \tag{B5a}$$

where $k = (2mE/\hbar^2)^{1/2}$, and with $\epsilon(q)$ given by Eq. (B2) one finds the complex turning point to be

$$q_t = q_0 + (q_{\max} - q_0)\left(\frac{E}{\lambda}\right)^{1/n} e^{i\pi/2n}. \tag{B5b}$$

With Eq. (B5), Eq. (B3) can be evaluated to give

$$R = \exp\left[-4k(q_{\max} - q_0)\left(\frac{E}{\lambda}\right)^{1/n} C_n\right], \tag{B6a}$$

where the constant C_n is

$$C_n = \sin\left(\frac{\pi}{2n}\right)\frac{\Gamma(1 + 1/n)\Gamma(3/2)}{\Gamma(1/n + 3/2)}. \tag{B6b}$$

Similarly, the WKB approximation for the probability that the same particle (i.e., incident from $q_1 < q_0$ and moving to the right) reaches the position $q_{\max}$, i.e., the *transmission probability* T, is

$$T = \left|\exp\left(i\int_{q_1}^{q_{\max}} dq\, k(q)\right)\right|^2 = \exp\left(-2\,\text{Im}\int_{q_0}^{q_{\max}} dq\, k(q)\right). \tag{B7}$$

With $\epsilon(q)$ given by Eq. (B2), and $k(q)$ by Eq. (B5a), this can be written as

$$T = \exp\left(-2k(q_{\max} - q_0) \times \text{Im}\int_0^1 dz(1 + iz^n\lambda/E)^{1/2}\right), \tag{B8}$$

which can be evaluated analytically only for the linear and quadratic cases. In general, one sees that the reflection and transmission probabilities of Eqs. (B6a) and (B8) depend only on two dimensionless parameters: S, the *strength* of the absorbing potential in units of E,

$$S = \frac{\lambda}{E}, \tag{B9a}$$

and W, the *width* of the absorbing region in units of k^{-1},

$$W = k(q_{\max} - q_0). \tag{B9b}$$

In terms of these dimensionless parameters, Eqs. (B6a) and (B8) read as

$$R = \exp\left(-4C_n\frac{W}{S^{1/n}}\right), \tag{B10a}$$

$$T = \exp\left(-2W\int_0^1 dz\,\text{Im}\,(1 + iSz^n)^{1/2}\right). \tag{B10b}$$

The physical considerations are that one wants R and T to be small, i.e., one wants no particles to be reflected by the absorbing potential ($R \ll 1$) and all the flux to be absorbed over the interval $(q_0, q_{\max})$ ($T \ll 1$). For example, if one wishes to have

$$R = T = 10^{-l}, \tag{B11}$$

where l is a predetermined tolerance, Eq. (B10) implies that

$$4C_n\frac{W}{S^{1/n}} \simeq 2.3l, \tag{B12a}$$

$$2WG_n(S) \simeq 2.3l, \tag{B12b}$$

where $G_n(S)$ is the function

$$G_n(S) = \int_0^1 dz\,\text{Im}\,(1 + iSz^n)^{1/2}. \tag{B13}$$

To solve Eqs. (B12) one first eliminates W to obtain a single equation for S

$$S^{1/n}G_n(S) = 2C_n, \tag{B14}$$

which is seen to be independent of the accuracy required in Eq. (B11) (i.e., how small R and T are required to be). After S is determined by solving Eq. (B14) (numerically), W is given by Eq. (B12a)

$$W = 2.3l\frac{S^{1/n}}{4C_n} \tag{B15}$$

and seen to be proportional to the "accuracy exponent" l.

Figure 11 shows the strength parameter S [Eq. (B14)] and the corresponding width parameter [Eq. (B15)] for $l = 3$, as a function of n, the power in Eq. (B2). Since one wishes the width of the absorbing potential to be as small as possible, Fig. 11 shows the optimum power to be $n \simeq 1.5$ and the corresponding (minimum) value of W to be approximately 2π. Thus, the width of the absorbing region needs to be at least 1 deBroglie wavelength,

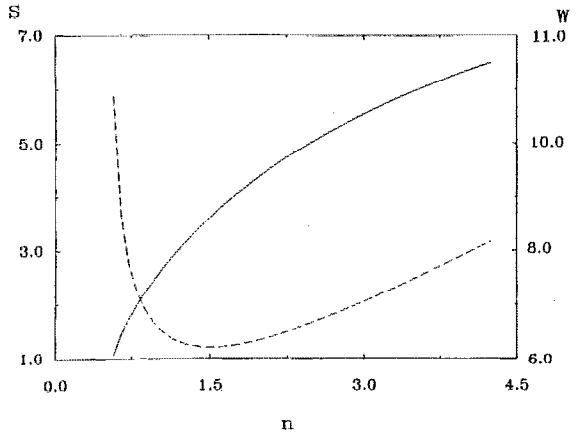

FIG. 11. The strength parameter (S) of Eq. (B14) (—) and the width parameter (W) of Eq. (B15) (---) as a function of n, the power in Eq. (B2).

$$q_{\max} - q_0 \geqslant \frac{W_{\min}}{k} \simeq \frac{2\pi}{k}, \tag{B16}$$

in order to achieve $T, R \leqslant 10^{-3}$.

The aforementioned WKB estimates may serve as qualitative guidelines for the choice of the absorbing potential parameters in the general multidimensional case. They should not, however, be interpreted quantitatively for other than a 1D problem with a power-law choice for $\epsilon(q)$, for two reasons. First, one wishes to apply the absorbing boundary conditions in regions where the physical potential differs from zero. Second, in practical systems more than a single channel is typically open and, therefore, the conditions of complete absorption and no reflection should be satisfied at more than a single translational energy. In practice, therefore, one needs to carry out convergence checks to determine the optimum form of the absorbing potential.

[1] T. Yamamoto, J. Chem. Phys. **33**, 281 (1960).
[2] (a) W. H. Miller, J. Chem. Phys. **61**, 1823 (1974); (b) W. H. Miller, S. D. Schwartz, and J. W. Tromp, *ibid.* **79**, 4889 (1983).
[3] (a) R. Jaquet and W. H. Miller, J. Phys. Chem. **89**, 2139 (1985); (b) K. Yamashita and W. H. Miller, J. Chem. Phys. **82**, 5475 (1985); (c) J. W. Tromp and W. H. Miller, J. Phys. Chem. **90**, 3482 (1986); (d) J. W. Tromp and W. H. Miller, Faraday Discuss. Chem. Soc. **84**, 441 (1987).
[4] R. E. Wyatt, Chem. Phys. Lett. **121**, 301 (1985).
[5] (a) T. P. Park and J. C. Light, J. Chem. Phys. **85**, 5870 (1986); (b) T. P. Park and J. C. Light, *ibid.* **88**, 4897 (1988); (c) T. P. Park and J. C. Light, *ibid.* **91**, 974 (1989); (d) M. Founargiotakis and J. C. Light, *ibid.* **93**, 633 (1990); (e) T. P. Park and J. C. Light, *ibid.* **94**, 2946 (1991).
[6] (a) G. Wahnstrom and H. Metiu, Chem. Phys. Lett. **134**, 531 (1982); J. Phys. Chem. **92**, 3240 (1988); (b) G. Wahnstrom, B. Carmeli, and H. Metiu, J. Chem. Phys. **88**, 2478 (1988).
[7] R. Lefebvre and N. Moiseyev, J. Chem. Phys. **93**, 7173 (1990).
[8] P. N. Day and D. G. Truhlar, J. Chem. Phys. **94**, 2045 (1991).
[9] W. H. Miller, J. Chem. Phys. **62**, 1899 (1975).
[10] (a) D. Thirumalai, B. C. Garrett, and B. J. Berne, J. Chem. Phys. **83**, 2972 (1985); (b) C. W. McCurdy and B. C. Garrett, *ibid.* **84**, 2630 (1986).
[11] T. Seideman and W. H. Miller, J. Chem. Phys. **95**, 1768 (1991).
[12] J. C. Light, I. P. Hamilton, and J. V. Lill, J. Chem. Phys. **82**, 1400 (1985).
[13] (a) Z. Bacic and J. C. Light, J. Chem. Phys. **85**, 4594 (1986); **86**, 3065 (1987); (b) R. M. Whitnell and J. C. Light, *ibid.* **90**, 1774 (1989); (c) S. E. Choi and J. C. Light, *ibid.* **92**, 2129 (1990).
[14] (a) J. V. Lill, G. A. Parker, and J. C. Light, Chem. Phys. Lett. **89**, 483 (1982); (b) J. V. Lill, G. A. Parker, and J. C. Light, J. Chem. Phys. **85**, 900 (1986).
[15] J. T. Muckerman, Chem. Phys. Lett. **173**, 200 (1990).
[16] D. T. Colbert and W. H. Miller, J. Chem. Phys. **96** (1992).
[17] A. Goldberg and B. W. Shore, J. Phys. B **11**, 3339 (1978).
[18] C. Leforestier and R. E. Wyatt, J. Chem. Phys. **78**, 2334 (1983).
[19] A. C. Reynolds, Geophysics **43**, 1099 (1978).
[20] (a) C. Cerjan, D. Kosloff, R. Kosloff, and T. Reshef, Geophysics **50**, 705 (1985); (b) R. Kosloff and D. Kosloff, J. Comput. Phys. **63**, 363 (1986).
[21] (a) D. Neuhauser and M. Baer, J. Chem. Phys. **90**, 4351 (1989); (b) D. Neuhauser and M. Baer, *ibid.* **91**, 4651 (1989); (c) D. Neuhauser M. Baer, R. S. Judson, and D. J. Kouri, *ibid.* **93**, 312 (1990); (d) D. Neuhauser and M. Baer, *ibid.* **92**, 3419 (1990); (e) M. Baer, C. Y. Ng, and D. Neuhauser, Chem. Phys. Lett. **169**, 534 (1990); (f) D. Neuhauser, M. Baer, and D. J. Kouri, J. Chem. Phys. **93**, 2499 (1990); (g) D. Neuhauser, *ibid.* **95**, 4927 (1991).
[22] See, for example, R. G. Newton, *Scattering Theory of Waves and Particles* (Springer-Verlag, Berlin, 1982).
[23] H. S. Johnston, *Gas Phase Reaction Rate Theory* (Ronald, New York, 1966), pp. 37–47.
[24] P. Siegbahn and B. Liu, J. Chem. Phys. **68**, 2457 (1978); D. G. Truhlar and C. J. Horowitz, *ibid.* **68**, 2566 (1978); **71**, 1514 (1979).
[25] (a) D. K. Bondi, D. C. Clary, J. N. L. Connor, B. C. Garret, and D. G. Truhlar, J. Chem. Phys. **76**, 4986 (1982); (b) D. K. Bondi and J. N. L. Connor, *ibid.* **82**, 4383 (1985).
[26] J. Z. H. Zhang (private communication).
[27] W. H. Miller and B. M. D. D. Jansen op de Haar, J. Chem. Phys. **86**, 6213 (1987).
[28] I. S. Gradshteyn and I. M. Ryzhik, *Table of Integrals, Series, and Products* (Academic, New York, 1965).